J. Fluid Mech. (2023), *vol*. 969, R1, doi:10.1017/jfm.2023.578

Attenuation of perturbation growth of single-mode SF_6–air interface through reflected rarefaction waves

Chenren Chen[1], **He Wang**[1], **Zhigang Zhai**[1,†] **and Xisheng Luo**[1]

[1]Advanced Propulsion Laboratory, Department of Modern Mechanics, University of Science and Technology of China, Hefei 230026, PR China

(Received 7 February 2023; revised 12 July 2023; accepted 12 July 2023)

Attenuation and even freeze-out (amplitude growth stagnation) of the perturbation amplitude growth of a shocked SF_6–air interface are first realized in shock-tube experiments through reflected rarefaction waves, which produce reverse baroclinic vorticity offsetting the vorticity deposited by the shock. A theoretical model is constructed to predict the perturbation growth after the impact of rarefaction waves, and seven possibilities of amplitude growth are analysed. Experimentally, a planar air–helium interface is used to produce reflected rarefaction waves. Through changing the perturbation wavelength and the time interval of two impacts, five experiments with specific initial conditions are carried out, and three different possibilities of perturbation growth attenuation are realized.

Key words: shock waves

1. Introduction

The Richtmyer–Meshkov (RM) instability (Richtmyer 1960; Meshkov 1969) occurs when a perturbed interface separating two fluids with different densities is impacted by a shock wave. The initial perturbation amplitudes continuously grow with time, which causes the formation of interpenetrating bubbles (lighter fluids penetrating into heavier ones) and spikes (heavier fluids penetrating into lighter ones), and eventually leads to the flow transitioning to turbulent mixing between the light and heavy components. The development of the RM instability is mainly driven by baroclinic vorticity produced by misalignment of the pressure and density gradients. In inertial confinement fusion (ICF) (Lindl *et al.* 2014), the development of the interface perturbation consumes a large amount of laser energy and impedes implosions. As a result, the RM instability is a

† Email address for correspondence: sanjing@ustc.edu.cn

significant obstacle to the realization of ICF and needs to be attenuated. If additional vorticity, which has the opposite sign to the original vorticity on the interface, is added to the single-shocked interface by a second wave impact, the perturbation growth can be degraded. This provides the possibility to attenuate the RM instability through a second wave impact.

The idea that the RM instability can be attenuated through a second shock impact was first proposed theoretically by Mikaelian (1985). If the amplitude growth rate induced by the second shock exactly cancels the growth rate caused by the first shock, the amplitude growth will stagnate, which is called freeze-out. A simple theoretical model was constructed by Mikaelian (1985) through superimposing the impulsive model (Richtmyer 1960) to predict the amplitude growth rate after two shock impacts. Through this model, various approaches to attenuate and even freeze the RM instability were theoretically proposed.

For a light–heavy interface, attenuation and freeze-out of the perturbation were realized through a weaker reflected shock in numerical simulations (Mikaelian 2010) and in shock-tube experiments (Chen *et al.* 2023). However, in a traditional ICF capsule, the incident shock always travels from the heavy fluid to the light one (Lindl *et al.* 2014). For a heavy–light interface, a reflected shock always enhances the perturbation growth (Guo *et al.* 2022). In the concept proposed by Mikaelian (1985), to attenuate the perturbation growth of a heavy–light interface after phase reversal, the second shock must propagate in the same direction as the first shock (two successive shock waves). Charakhch'yan (2000, 2001) numerically verified that attenuation and freeze-out of a heavy–light perturbation growth can be realized through the impacts by two successive shock waves. Experimentally, however, it is difficult to generate and precisely control two successive shock waves in a conventional shock tube. Therefore, experimental studies on attenuation and freeze-out of a heavy–light interface perturbation are rare.

When reflected rarefaction waves move from light gas to heavy gas through a shocked interface, baroclinic vorticity of the opposite sign to that deposited by the incident shock will be produced on the shocked heavy–light interface. This provides a possibility to attenuate the RM instability of a heavy–light perturbation through the impact of reflected rarefaction waves. However, the impact of rarefaction waves will generally introduce the Rayleigh–Taylor (RT) instability (Rayleigh 1883; Taylor 1950), which complicates the flow. Previous studies mainly focused on the RT instability induced by rarefaction waves (Morgan, Likhachev & Jacobs 2016; Morgan *et al.* 2018), and the RM instability induced by rarefaction waves is rarely investigated in shock-tube experiments.

In this work, the perturbation development of a single-mode SF_6–air interface accelerated by an incident shock and its reflected rarefaction waves is investigated. A planar air–helium gas interface is used to produce reflected rarefaction waves. The duration of the reflected rarefaction waves interacting with the shocked interface is assumed to be short enough to ignore the RT instability. Through manipulating the perturbation wavelength and the time interval of the two impacts, three different behaviours of the perturbation growth attenuation after the rarefaction waves impact are experimentally realized. We shall first construct a model to predict the amplitude growth rate after the rarefaction waves impact. Then, corresponding experiments are designed according to the model. It will be shown that the amplitude growth is attenuated after the impact of rarefaction waves, and freeze-out is achieved under some designed conditions.

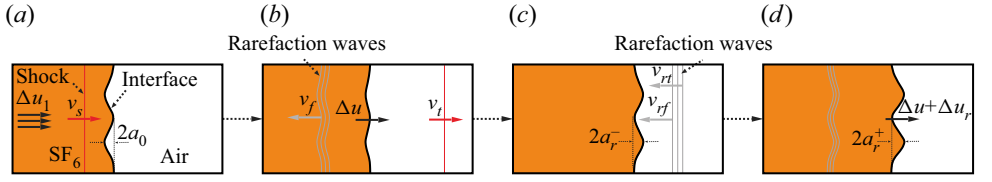

Figure 1. Schematics showing the interaction processes of the incident shock and reflected rarefaction waves with a single-mode SF_6–air interface: (*a*) before and (*b*) after the incident shock impact; and (*c*) before and (*d*) after the reflected rarefaction waves impact. Here a_0 is the initial perturbation amplitude; v_s, v_t and v_f are the velocities of the incident shock, the transmitted shock and the front of the single-mode reflected rarefaction waves during the interaction of the incident shock with the SF_6–air interface; Δu (Δu_r) and Δu_1 are the jump velocity of the interface induced by the incident shock (rarefaction waves) and the heavy-fluid velocity caused by the incident shock; a_r^- (a_r^+) is the perturbation amplitude just before (after) the rarefaction waves impact; and v_{rf} (v_{rt}) is the velocity of the rarefaction waves front (tail) relative to the gas before the rarefaction waves.

2. Theoretical analysis

There are three assumptions for theoretical analysis. First, the wavenumber (k) and amplitude (a_r^-) of the perturbation satisfy the small-perturbation hypothesis when the rarefaction waves arrive, i.e. $ka_r^- < 1$. Second, the amplitude growth rates induced by the incident shock and the rarefaction waves follow the linear superposition principle (Mikaelian 1985), namely, $V_2 = V_i + V_r$, where V_2 is the amplitude growth rate after the rarefaction waves impact, V_i is the growth rate caused by the incident shock just before the rarefaction waves arrive and V_r is the linear growth rate induced by the rarefaction waves. Third, the duration of the planar rarefaction waves interacting with the shocked interface is short enough that the RT instability (Rayleigh 1883; Taylor 1950) induced by the rarefaction waves can be ignored.

Sketches showing the interactions of a planar shock and reflected rarefaction waves with a single-mode SF_6–air interface are presented in figure 1. As the incident shock impacts the interface, the transmitted shock and the reflected rarefaction waves are generated, as shown in figure 1(*b*). To predict the amplitude development of a single-mode perturbation induced by a planar shock wave, the nonlinear model proposed by Zhang & Guo (2016) (the ZG model) is adopted since it has been widely verified in previous work (Liu *et al.* 2018; Guo *et al.* 2022). The ZG model can be described as

$$V_i = V_i^{ZG}(t) = \frac{1}{2}[V_b^{ZG}(t) + V_s^{ZG}(t)], \quad V_{b/s}^{ZG}(t) = -\frac{|V_i^0|}{1 + \theta k |V_i^0| t}. \tag{2.1a,b}$$

Here $V_{b/s}$ is the amplitude growth rate of the bubble/spike, where the minus sign denotes that the heavy–light perturbation growth induced by a shock has the opposite direction to the phase of perturbation before impact (Meyer & Blewett 1972; Guo *et al.* 2022); V_i^0 is the linear amplitude growth rate of the heavy–light perturbation; and

$$\theta = \frac{3}{4}\frac{(1+A^+)(3+A^+)}{[3+A^+ + \sqrt{2}(1+A^+)^{1/2}]}\frac{[4(3+A^+) + \sqrt{2}(9+A^+)(1+A^+)^{1/2}]}{[(3+A^+)^2 + 2\sqrt{2}(3-A^+)(1+A^+)^{1/2}]} \tag{2.2}$$

is a function of the post-shock Atwood number ($A^+ = (\rho_2^+ - \rho_1^+)/(\rho_2^+ + \rho_1^+)$, with ρ_1^+ and ρ_2^+ being the densities of the heavy and light fluids on both sides of the perturbed interface after the incident shock impact), with positive Atwood number for bubble and its negative counterpart for spike; θ represents the effect of Atwood number on the asymptotic growth rate of the perturbation amplitude.

To accurately predict V_i^0, the irrotational model proposed by Wouchuk & Nishihara (1997) (the WN model) is used, which can be expressed as

$$V_i^0 = ka_0 \frac{\rho_2^+ \Delta u \left(1 - \dfrac{v_t}{v_s}\right) + \rho_1^+ (\Delta u_1 - \Delta u)\left(1 + \dfrac{v_f}{v_t}\right)}{\rho_1^+ + \rho_2^+}. \tag{2.3}$$

Here a_0 is the initial amplitude of the perturbation; v_s, v_t and v_f are the velocities of the incident shock, the transmitted shock and the front of the single-mode reflected rarefaction waves during the interaction of the incident shock with the SF_6–air interface; and Δu and Δu_1 are the jump velocity of the interface induced by the incident shock and the heavy-fluid velocity caused by the incident shock, respectively. These parameters in (2.3) can be calculated using one-dimensional (1-D) gas dynamics theory by providing the initial parameters. Through the ZG model, the perturbation amplitude just before the arrival of the front of planar reflected rarefaction waves can be calculated, i.e. $a_r^- = a_0 C_1 + \int_0^{\Delta t} V_i^{ZG}(t)\,\mathrm{d}t$, in which $C_1 = 1 - \Delta u/v_s$ is the shock compression factor (Meshkov 1969) and Δt is the time interval between impacts of the incident shock and the planar rarefaction waves.

After the planar reflected rarefaction waves impact the perturbed air–SF_6 interface, reflected and transmitted rarefaction waves are generated, as shown in figure 1(*d*), and the perturbation amplitude grows linearly in the RM instability flow. Note that the WN model is not appropriate to predict the growth rate induced by the rarefaction waves because it was constructed based on the fact that the transmitted wave is a shock.

In this work, the modified impulsive model proposed by Vandenboomgaerde, Mügler & Gauthier (1998) (the Van model) is used to accurately predict the linear growth rate (V_r) of a single-mode heavy–light perturbation accelerated by rarefaction waves (Zhou *et al.* 2021), and the Van model can be expressed as

$$V_r = -k \frac{a_r^- A^+ + a_r^+ A^r}{2} \Delta u_r. \tag{2.4}$$

Here Δu_r is the interface velocity jump induced by the rarefaction waves; and a_r^+ (A^r) is the perturbation amplitude (Atwood number) just after the rarefaction waves collide with the shocked interface. The perturbation amplitude can be described as $a_r^+ = Ra_r^-$, with $R = 1 + \Delta u_r/(v_{rf} + v_{rt})$ being the rarefaction factor and v_{rf} (v_{rt}) being the velocity of the rarefaction waves front (tail) relative to the gas before the rarefaction waves. By solving the 1-D gas dynamics equations after providing the intensities of the planar shock and rarefaction waves and the initial gas parameters, the parameters in (2.4) can be calculated.

According to the theoretical analysis, V_2 can be accurately predicted if the initial parameters are provided. There are seven possibilities for the perturbation development after the rarefaction waves impact, as presented in table 1, and the details of these possibilities are presented as follows. For convenient discussion, we assume $a_0 > 0$, and therefore $V_i^0 < 0$ and $V_i < 0$.

Possibility I ($V_2 < V_i < 0$): The impact of rarefaction waves occurs before the phase reversal of the perturbation is completed. The perturbation growth induced by the rarefaction waves (V_r) has the same direction as that induced by the shock (V_i). Thus, V_2 and V_i have the same sign and the rarefaction waves impact accelerates the perturbation growth.

Possibility II ($V_2 = V_i < 0$): The rarefaction waves reach the balanced position of the shocked interface at the moment when the phase reversal is just finished, i.e. the rarefaction

Possibility	Rarefaction waves impact	Relation between growth rates	Growth after second impact
I	before phase reversal	$V_2 < V_i < 0$	faster growth
II	phase reversal just finished	$V_2 = V_i < 0$	unaffected
III	after phase reversal	$V_i < V_2 < 0$	slower growth
IV	after phase reversal	$V_i < V_2 = 0$	freeze-out
V	after phase reversal	$-V_i > V_2 > 0$	slower growth
VI	after phase reversal	$-V_i = V_2 > 0$	growth reversal
VII	after phase reversal	$V_2 > -V_i > 0$	faster growth

Table 1. The classification of seven possibilities.

waves impact a flat interface ($a_r^- = 0$). Under the hypotheses above (weak rarefaction waves and small perturbations), the density field near the interface before and after the rarefaction waves impact can be approximately regarded as uniform. Consequently, the rarefaction waves have no effect on the perturbation growth ($V_r = 0$). This specific condition is called the 'acceleration line' in this work.

Possibility III ($V_i < V_2 < 0$): The rarefaction waves impact occurs when the phase reversal has finished, i.e. $a_r^- < 0$, and V_r has the opposite direction to V_i. However, a_r^- is small, and $|V_r| < |V_i|$. After the rarefaction waves impact, the perturbation growth rate is attenuated but the perturbation amplitude continues to grow in the same direction as the interface before rarefaction waves impact.

Possibility IV ($V_i < V_2 = 0$): V_r and V_i have the same magnitudes but different directions, and they almost offset each other. After the rarefaction waves impact, the velocity field in the vicinity of the interface is nearly uniform, and freeze-out of amplitude growth is realized. This specific condition is called the 'freeze-out line' in this work.

Possibility V ($-V_i > V_2 > 0$): In this situation, a_r^- is high enough, and V_r has a slightly larger magnitude than V_i but the opposite direction to V_i. After the impact of rarefaction waves, the perturbation growth rate is weakened ($V_2 < -V_i$), and the perturbation amplitude first decreases with a smaller rate than that before the rarefaction waves impact. After the second phase reversal is finished, the perturbation amplitude continues to grow and has the same phase as the initial amplitude (a_0).

Possibility VI ($-V_i = V_2 > 0$): Here, V_r is twice V_i in magnitude. Thus, V_2 has the same magnitude as V_i but the opposite direction to V_i. Although the rarefaction waves impact fails to attenuate the perturbation growth rate, the perturbation amplitude decreases first in time with the same rate as that before the rarefaction waves impact. This specific condition is called the 'reversal acceleration line' in this work.

Possibility VII ($V_2 > -V_i > 0$): V_r is more than twice V_i in magnitude. The perturbation amplitude decreases in time until the second phase reversal occurs. The rarefaction waves impact accelerates the perturbation growth but reverses the growth direction.

3. Experimental method

In this work, a planar air–helium gas interface is used to produce weak reflected rarefaction waves. As shown in figure 2(*a*,*b*), there are two interfaces, a perturbed one and a planar one. The single-mode perturbed interface (II) separates air (in space B) from SF_6 (in space A and driven section), and the planar interface (AI) separates air (in space B) from helium (in space C). The distance between II and AI is defined as L_0, which has a linear

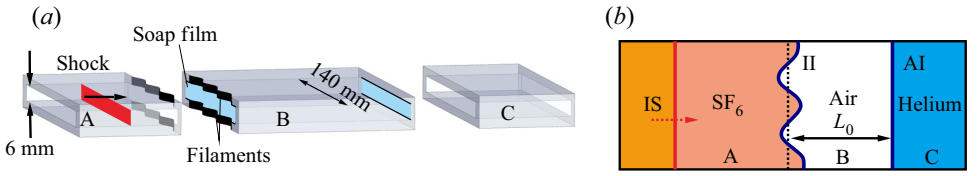

Figure 2. Schematics of the soap-film interface generation (*a*) and initial configuration studied (*b*). Here AI is the auxiliary air–helium interface; II is the initial SF_6–air interface; IS is the incident shock; and L_0 is the initial distance between the average positions of II and AI.

relationship with Δt when the other initial parameters are fixed. The linear relationship between L_0 and Δt can be solved through 1-D gas dynamics equations. The determination of L_0 is important, because a smaller (larger) L_0 will result in a smaller (larger) amplitude of the interface at the arrival of the rarefaction waves and consequently a smaller (larger) amplitude growth rate induced by the rarefaction waves. In other words, the amplitude growth rate induced by the rarefaction waves can be manipulated through changing L_0, and different attenuation behaviours may be achieved.

The soap-film technique (Liu *et al.* 2018) is used to create the initial perturbed and planar interfaces. After the soap-film interfaces are formed, SF_6 is pumped into the driven section and space A, and helium is pumped into space C. For all experimental runs, the inflation rate and duration are the same to ensure similar volume fractions of SF_6 and helium in the spaces as far as possible. Note that the value of L_0 will alter the volume of space C. In experiments, the inflation rate and duration are determined to ensure the helium concentration of about 100 % when the volume of space C is the largest. However, because helium diffuses much faster, its concentration cannot be 100 % when the incident shock impacts. The gas concentration is determined by comparing the velocities of the incident shock and the transmitted shock, and the interface velocity jump measured from experiments, with those predicted from 1-D gas dynamics theory.

The experiments are conducted in a horizontal shock tube (Liu *et al.* 2018; Guo *et al.* 2022), and the Mach number of the incident planar shock moving in SF_6 is 1.37 ± 0.01. The post-shock flow field is recorded by high-speed schlieren photography. The frame rate of the high-speed video camera (FASTCAM SA-Z, Photron Ltd) is 50 400 frames per second and the exposure time is 0.36 μs. The spatial resolution of the schlieren image is 0.25 mm pixel^{-1}. The ambient pressure and temperature are 101.3 ± 0.1 kPa and 295 ± 1.5 K.

4. Results and discussion

4.1. *Undisturbed case*

The developments of the undisturbed II after shock and rarefaction waves impacts are investigated first, and the experimental schlieren images with L_0=144 mm are presented in figure 3(*a*). The initial time is defined as the moment when the incident shock (IS) meets II, and similarly hereinafter. As IS impinges upon II, a transmitted shock wave (TS) and a shocked SF_6–air interface (SI) are formed (96 μs). Then TS impacts the auxiliary air–helium interface (AI), which produces a shocked air–helium interface (SAI) and planar rarefaction waves moving upstream (394 μs). Note that the rarefaction waves in air cannot be captured due to their weak intensity. After the rarefaction waves impact SI, transmitted rarefaction waves (TRW) moving in SF_6 and the interface RSI are generated (632 μs). Subsequently, RSI moves downstream (969 μs). Note that, due to the size

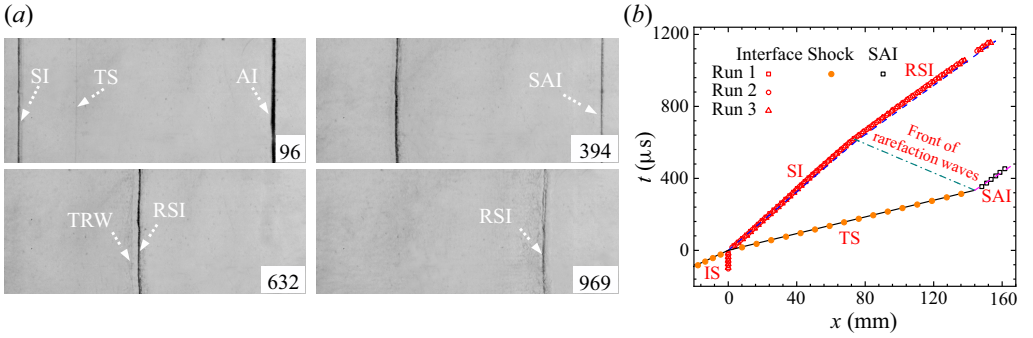

Figure 3. Evolution of an undisturbed SF_6–air interface accelerated by a plane shock and rarefaction waves (*a*) and the trajectories of the interface and waves (*b*). Here SI is the shocked SF_6–air interface; SAI is the shocked auxiliary air–helium interface; TS is the transmitted shock; RSI is the interface after rarefaction waves impact; TRW is the transmitted rarefaction waves; and x is the distance of the evolving interface from the initial position of II. The symbols (lines) represent the experimental (theoretical) results.

M_s	$\varphi(SF_6)$	φ(air)	φ(helium)	A^+	A^r	v_s	v_t	v_f	Δu	Δu_1	Δu_r	Δu_{aui}
1.37	0.63	1.00	0.81	−0.59	−0.58	226.2	431.2	72.9	123.2	99.7	22.9	158.7

Table 2. Experimental parameters: M_s is the incident shock Mach number; $\varphi(SF_6)$, φ(air) and φ(helium) are the volume fractions of SF_6 in space A, air in space B and helium in space C, respectively; A^+ and A^r are the post-shock and post-rarefaction waves Atwood numbers; and Δu_{aui} is the jump velocity of the air–helium interface induced by the transmitted shock. The unit of velocity is m s^{-1}.

limitation of the observation window, the developments of these two interfaces cannot be captured simultaneously by the camera during the whole experimental duration, and only the developments of the perturbed SF_6–air interface are highlighted hereinafter.

The trajectories of the shock waves and the two interfaces extracted from the experimental schlieren images are shown in figure 3(*b*). Three experimental runs are performed, and the interface trajectories for these runs are nearly the same. According to the parameters in table 2, the theoretical trajectories of the shock waves and interfaces are also plotted for comparison. Good agreement between experiments and predictions is achieved, verifying the good repeatability and reliability of the experiments. As a result, the parameters in table 2 are considered as the initial parameters in the following experiments. Based on the parameters in table 2, the relationship between L_0 (mm) and Δt (μs) can be described as $L_0 = 0.237\Delta t$.

In the following studies, we focus on the realization of the perturbation growth attenuation (possibilities III–V). Three kinds of single-mode SF_6–air interfaces with different λ are considered. According to the experimental parameters in undisturbed runs, five different L_0, as presented in table 3, are designed to realize different attenuations of the perturbation growth. Three experiments (cases 1–3) are performed by changing L_0 to verify different possibilities of the perturbation growth attenuation for the same initial interface condition, and two additional experiments (cases 4 and 5) are performed to achieve freeze-out of the perturbation with different initial interface conditions.

For each case, at least three successful experimental runs are performed to ensure the repeatability of experiments. The velocities of the incident shock (226.2 ± 1.0 m s^{-1}), the transmitted shock (431.2 ± 1.0 m s^{-1}) and the auxiliary air–helium interface

Case	L_0 (mm)	a_0 (mm)	ka_0	ka_r^-	λ (mm)	V_i^t (m s^{-1})	V_i^e (m s^{-1})	Possibility
1	149	0.64	0.10	−0.38	40	−4.11	-4.23 ± 0.13	III
2	79	0.64	0.10	−0.20	40	−3.77	-3.75 ± 0.13	V
3	109	0.64	0.10	−0.28	40	−4.03	-4.06 ± 0.06	IV
4	82	0.48	0.10	−0.28	30	−4.03	-4.09 ± 0.12	IV
5	164	0.95	0.10	−0.28	60	−4.03	-4.08 ± 0.09	IV

Table 3. Interface parameters and L_0 in perturbed cases. Here k and λ are the perturbation wavenumber and wavelength; and V_i is the growth rate of amplitude just before the reflected rarefaction waves arrival. The superscripts 't' and 'e' denote theoretical and experimental results.

(158.7 ± 1.0 m s^{-1}) for the different cases are nearly the same. Based on the 1-D gas dynamics theory, the duration of the rarefaction waves interacting with the perturbed interface can be calculated as 13–28 μs in different cases, and the jump velocity induced by the rarefaction waves is relatively small ($\Delta u_r \sim 20$ m s^{-1}). Comparing with the previous work on the interaction of the rarefaction waves with a single-mode interface (Liang *et al.* 2020), it is reasonably assumed that the interaction duration in this work is short enough to ignore the RT instability caused by the rarefaction waves.

4.2. *Single-mode cases*

When the initial experimental parameters and shock intensity are fixed, the initial interface shape and L_0 can determine the possibilities of the perturbation growth. In this work, the initial dimensionless amplitude ka_0 is 0.1 and remains constant. The different possibilities of attenuation are achieved through varying λ and L_0. Note that changing λ instead of ka_0 is more convenient and effective. For example, when $\lambda = 40$ mm and $ka_0 = 0.1$, L_0 is calculated to be about 109 mm to achieve freeze-out of RSI perturbation. If λ is changed to 30 mm while $ka_0 = 0.1$ remains fixed, L_0 becomes 82 mm for achieving freeze-out. However, if ka_0 is changed to 0.2 while λ is fixed as 40 mm, L_0 is about 105 mm for achieving freeze-out.

Figure 4 shows the distributions of the perturbation growth possibilities after the reflected rarefaction waves impact in the (λ, L_0) domain. As analysed in § 2, seven different possibilities are classified by three specific lines. In the following studies, we first fix λ as 40 mm but change L_0 (cases 1–3 in table 3) to achieve three possibilities (III–V). Then, two additional cases (cases 4 and 5 in table 3) with different λ are chosen to verify that the model proposed can accurately predict the freeze-out conditions (possibility IV). The distributions of these five cases in the (λ, L_0) domain are shown in figure 4.

Typical schlieren images of the SF_6–air interfaces accelerated by the incident shock and the reflected rarefaction waves for cases 1–5 are provided in figure 5. Taking case 1 as an example, when IS interacts with II, a transmitted shock (TS) and reflected single-mode rarefaction waves (RW_1) are generated (87 μs). The shocked II (SI) moves downstream and phase reversal occurs. Because the amplitude of II is small, TS quickly recovers to a planar shock. Subsequently, TS impacts AI, generating a transmitted shock moving in helium and reflected rarefaction waves moving in air. These waves are invisible in air due to their weak intensities (326 μs). After the rarefaction waves collide with SI, transmitted rarefaction waves (TRW) moving in SF_6 can be observed (365 μs), and the perturbation amplitude of RSI grows continuously (544–1079 μs). In case 2, after the rarefaction waves impact, it is clear that the perturbation amplitude of RSI reduces (694–1190 μs). In cases

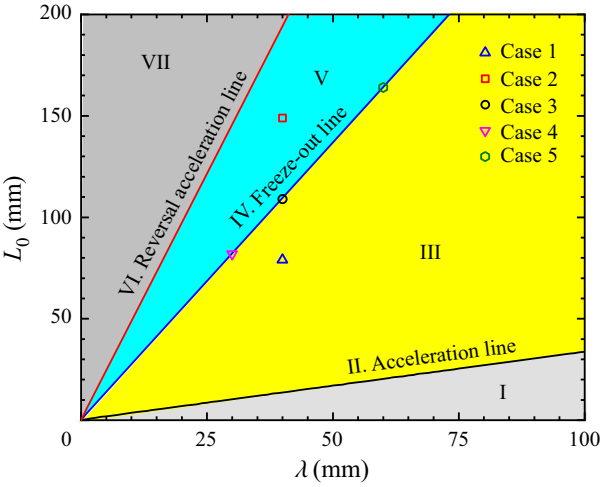

Figure 4. Distributions of seven possibilities of the perturbation growth after the impact of reflected rarefaction waves in the (λ, L_0) domain.

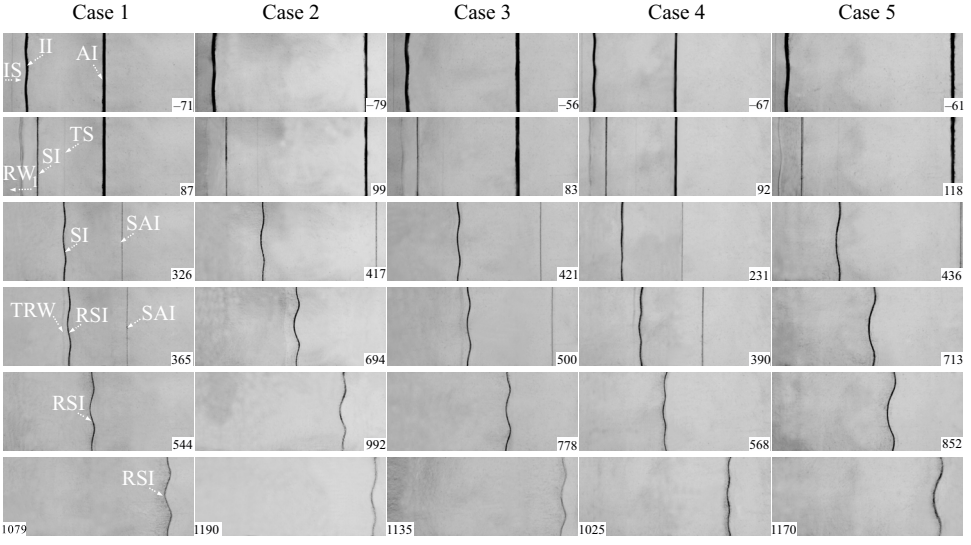

Figure 5. Typical schlieren images showing the interface evolution and wave patterns before and after the impact of rarefaction waves for cases 1–5.

3–5, after the rarefaction waves impact, the perturbation amplitudes of RSI are almost unchanged, and freeze-out is achieved.

The temporal variations of the dimensionless amplitude for cases before and after the impact of rarefaction waves are plotted in figure 6(*a*). The time is normalized as $\tau = kV_0^e(t - t^*)$, where V_0^e is the experimental linear growth rate of the SI amplitude and t^* is the time when the linear growth of the SI amplitude starts (compression phase ends). The growth rate V_0^e is 5.01 ± 0.12 m s^{-1} for all cases in this work and V_i^0 is calculated through the WN model to be 5.05 m s^{-1}. The amplitude is scaled as $\alpha = k(a - a^*)$, where a^* is the amplitude of SI at $t = t^*$, which differs from the initial amplitude. As shown in

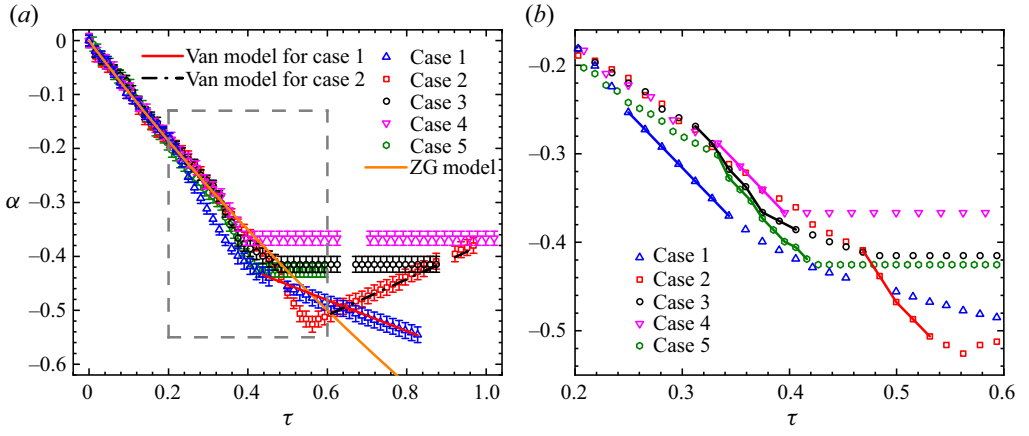

Figure 6. (*a*) Temporal variations of the dimensionless perturbation amplitude before and after the rarefaction waves impact for cases 1–5. (*b*) Zoomed-in image showing the stretching effect of the rarefaction waves, as represented by the solid lines.

figure 6(*a*), before the rarefaction waves impact, the data for different cases collapse well. The amplitude growth rates before the rarefaction waves can be accurately predicted by the ZG model (Zhang & Guo 2016), as shown in table 3.

After the rarefaction waves impact, the interface experiences a rarefaction process, and the amplitude of RSI first increases rapidly for a short time. To clearly show the stretching effect of the rarefaction waves, the results shortly before and after the rarefaction waves impact are zoomed in, as indicated in figure 6(*b*), in which the stretching effect of the rarefaction waves is represented by solid lines. Then after the start-up process (Lombardini & Pullin 2009), the amplitude growth is attenuated in all cases. In case 1, the amplitude of RSI continues to grow but its growth rate ($V_2^t = -1.44$ m s^{-1} and $V_2^e = -1.41 \pm 0.04$ m s^{-1}, where the superscripts 't' and 'e' denote theoretical and experimental results) is smaller than the counterparts just before the rarefaction waves impact ($V_i^t = -4.11$ m s^{-1} and $V_i^e = -4.23 \pm 0.13$ m s^{-1}). In case 2, before the second phase reversal is finished, the amplitude of RSI decreases with a smaller rate ($V_2^t = 1.68$ m s^{-1} and $V_2^e = 1.61 \pm 0.05$ m s^{-1}) than V_i ($V_i^t = -3.77$ m s^{-1} and $V_i^e = -3.75 \pm 0.13$ m s^{-1}). The linear growth rates after the rarefaction waves impact in these two cases are well predicted by the Van model, as given in figure 6(*a*). In cases 3–5, the amplitude growth of RSI almost stagnates, and freeze-out of amplitude growth of single-mode SF_6–air perturbations with different wavelengths is realized in shock-tube experiments.

In summary, attenuation and even freeze-out of amplitude growth of a shocked single-mode SF_6–air interface can be realized through the second impact by reflected rarefaction waves, and the relationship among initial parameters for attenuating the amplitude growth can be accurately predicted by theoretical models.

5. Conclusions

Attenuation and freeze-out of amplitude growth of a shocked single-mode SF_6–air interface is first realized through the impact of reflected rarefaction waves both theoretically and experimentally.

Theoretically, the ZG model (Zhang & Guo 2016) is used to predict the amplitude growth before the rarefaction waves impact and the Van model (Vandenboomgaerde *et al.* 1998) to predict perturbation growth induced by the rarefaction waves. Based on the

linear superposition principle, seven possibilities of perturbation growth are classified. It is found that the reflected rarefaction waves can enhance, attenuate and even freeze the interfacial instability. The possibility can be flexibly changed through varying the time interval between the two impacts and the perturbation wavelength by fixing other initial parameters.

Experimentally, a planar air–helium interface is used to produce the reflected rarefaction waves, and the soap-film technique is used to create the initially perturbed and undisturbed interfaces. Five experiments with different initial conditions are carried out, and the schlieren images show that, after the reflected rarefaction waves impact, the amplitude growth of single-mode heavy–light perturbation can be weakened or frozen-out, as accurately predicted by models.

These findings may be helpful for better understanding how to suppress hydrodynamic instabilities in ICF. Note that this work only considers the manipulation of single-mode interface perturbation growth. In a following work, the manipulation of a multimode interface perturbation growth, which is more desirable in ICF, will be considered.

Funding. This work was supported by the National Natural Science Foundation of China (nos 12022201, 91952205 and 12102425) and Youth Innovation Promotion Association CAS.

Declaration of interests. The authors report no conflict of interest.

Author ORCIDs.
He Wang https://orcid.org/0000-0002-6497-6673;
Zhigang Zhai https://orcid.org/0000-0002-0094-5210;
Xisheng Luo https://orcid.org/0000-0002-4303-8290.

References

Charakhch'yan, A.A. 2000 Richtmyer–Meshkov instability of an interface between two media due to passage of two successive shocks. *J. Appl. Mech. Tech. Phys.* **41**, 23–31.

Charakhch'yan, A.A. 2001 Reshocking at the non-linear stage of Richtmyer–Meshkov instability. *Plasma Phys. Control. Fusion* **43**, 1169–1179.

Chen, C., Xing, Y., Wang, H., Zhai, Z. & Luo, X. 2023 Freeze-out of perturbation growth of single-mode helium-air interface through reflected shock in Richtmyer–Meshkov flows. *J. Fluid Mech.* **956**, R2.

Guo, X., Cong, Z., Si, T. & Luo, X. 2022 Shock-tube studies of single- and quasi-single-mode perturbation growth in Richtmyer–Meshkov flows with reshock. *J. Fluid Mech.* **941**, A65.

Liang, Y., Zhai, Z., Luo, X. & Wen, C. 2020 Interfacial instability at a heavy/light interface induced by rarefaction waves. *J. Fluid Mech.* **885**, A42.

Lindl, J., Landen, O., Edwards, J., Moses, E. & NIC team 2014 Review of the national ignition campaign 2009–2012. *Phys. Plasmas* **21**, 020501.

Liu, L., Liang, Y., Ding, J., Liu, N. & Luo, X. 2018 An elaborate experiment on the single-mode Richtmyer–Meshkov instability. *J. Fluid Mech.* **853**, R2.

Lombardini, M. & Pullin, D.I. 2009 Startup process in the Richtmyer–Meshkov instability. *Phys. Fluids* **21**, 044104.

Meshkov, E.E. 1969 Instability of the interface of two gases accelerated by a shock wave. *Fluid Dyn.* **4**, 101–104.

Meyer, K.A. & Blewett, P.J. 1972 Numerical investigation of the stability of a shock-accelerated interface between two fluids. *Phys. Fluids* **15**, 753–759.

Mikaelian, K.O. 1985 Richtmyer–Meshkov instabilities in stratified fluids. *Phys. Rev.* A **31**, 410–419.

Mikaelian, K.O. 2010 Analytic approach to nonlinear hydrodynamic instabilities driven by time-dependent accelerations. *Phys. Rev.* E **81**, 016325.

Morgan, R.V., Cabot, W.H., Greenough, J.A. & Jacobs, J.W. 2018 Rarefaction-driven Rayleigh–Taylor instability. Part 2. Experiments and simulations in the nonlinear regime. *J. Fluid Mech.* **838**, 320–355.

Morgan, R.V., Likhachev, O.A. & Jacobs, J.W. 2016 Rarefaction-driven Rayleigh–Taylor instability. Part 1. Diffuse-interface linear stability measurements and theory. *J. Fluid Mech.* **791**, 34–60.

RAYLEIGH, LORD 1883 Investigation of the character of the equilibrium of an incompressible heavy fluid of variable density. *Proc. Lond. Math. Soc.* **14**, 170–177.

RICHTMYER, R.D. 1960 Taylor instability in shock acceleration of compressible fluids. *Commun. Pure Appl. Maths* **13**, 297–319.

TAYLOR, G. 1950 The instability of liquid surfaces when accelerated in a direction perpendicular to their planes. I. *Proc. R. Soc. Lond.* A **201**, 192–196.

VANDENBOOMGAERDE, M., MÜGLER, C. & GAUTHIER, S. 1998 Impulsive model for the Richtmyer–Meshkov instability. *Phys. Rev.* E **58**, 1874–1882.

WOUCHUK, J.G. & NISHIHARA, K. 1997 Asymptotic growth in the linear Richtmyer–Meshkov instability. *Phys. Plasmas* **4**, 1028–1038.

ZHANG, Q. & GUO, W. 2016 Universality of finger growth in two-dimensional Rayleigh–Taylor and Richtmyer–Meshkov instabilities with all density ratios. *J. Fluid Mech.* **786**, 47–61.

ZHOU, Y., *et al.* 2021 Rayleigh–Taylor and Richtmyer–Meshkov instabilities: a journey through scales. *Physica* D **423**, 132838.